Crystallographic and docking (Cathepsins B, K, L and S) studies on bioactive halotelluroxetanes

Ignez Caracelli,*,I Stella H. Maganhi,II Josiane de Oliveira Cardoso,I Rodrigo L. O. R. Cunha,III Mauricio Angel Vega-Teijido,‡,IV Julio Zukerman-Schpector IV and Edward R. T. Tiekink*,V

I BioMat, Departamento de Física, Universidade Federal de São Carlos, C.P. 676, São Carlos, SP, 13565-905, Brazil

II BioMat, Programa de Pós-graduação em Biotecnologia, Universidade Federal de São Carlos, C.P. 676, São Carlos, SP, 13565-905, Brazil

III Center of Natural Sciences and Humanities, Federal University of ABC, Santo André, São Paulo 09210-180, Brazil

IV Laboratório de Cristalografia, Estereodinâmica e Modelagem Molecular, Departamento de Química, Universidade Federal de São Carlos, C.P. 676, São Carlos, SP, 13565-905, Brazil

V Research Centre for Crystalline Materials, School of Science and Technology, Sunway University, 47500 Bandar Sunway, Selangor Darul Ehsan, Malaysia

Received; accepted

Keywords: Halotelluroxetanes / DFT / docking in Cathepsins / crystal structure analysis / X-ray diffraction

Abstract. The molecular structures of the halotelluroxetanes p-$MeOC_6H_4Te(X)[C(=C(H)X')C(CH_2)_nO]$, *X* = *X′* = Cl and n = 6 (**1**) and *X* = Cl, *X′* = Br and n = 5 (**4**), show similar binuclear aggregates sustained by $\{\cdots Te–O\}_2$ cores comprising covalent Te–O and secondary Te···O interactions. The resulting C_2ClO_2(lone-pair) sets define pseudo-octahedral geometries. In each structure, C–X···π(arene) interactions lead to supramolecular layers. Literature studies have shown these and related compounds (i.e. **2**: *X* = *X′* = Cl and n = 5; **3**: *X* = *X′* = Br and n = 5) to inhibit Cathepsins B, K, L and S to varying extents. Molecular docking calculations have been conducted on ligands (i.e. cations derived by removal of the tellurium-bound X atoms) **1'-3'** (note **3'** = **4'**) enabling correlations between affinity for sub-sites and inhibition. The common feature of all docked complexes was the formation of a Te–S covalent bond with cysteine residues, the relative stability of the ligands with an E-configuration and the formation of a C–O···π interaction with the phenyl ring; for **1'** the Te–S covalent bond was weak, a result correlating with its low inhibition profile. At the next level differences are apparent, especially with respect to the interactions formed by the organic-ligand-bound halides. While these atoms do not

form specific interactions in Cathepsins B and K, in Cathepsin L, these halides are involved in C–O···X halogen bonds.

* Correspondence authors: ignez@df.ufscar.br (I.C.); edwardt@sunway.edu.my (E.R.T.T.)
‡ Present address: Computational Chemistry and Biology Group—CCBG, DETEMA, Facultad de Química-Universidad de la República, CC1157 Montevideo Uruguay

Introduction

Since the discovery of selenium as a component of glutathione peroxidase [1, 2] and of the 21st amino acid, selenocysteine [3, 4], selenium compounds have been increasingly investigated as potential therapeutic agents against a range of diseases [5-10]. Due to the chemical similarities to tellurium, selenium's heavier congener, tellurium compounds have also attracted interest in the pharmaceutical context [11, 12]. Thus, tellurium compounds have shown promise since they are an immunomodulator in organisms [13] and display anti-oxidant [14-16], anti-parasitic [17, 18] and anti-inflammatory [19] activities, are known to be neuroprotective [20, 21] and have potential to be developed as anti-cancer agents [22-24]. The most notable tellurium compound that exerts biological activity is found in the salt ammonium trichlorido (dioxyethylene-O,O')tellurate, known as AS-101 (Figure 1a) [25]. This low-molecular weight organotellurate is a potent immunomodulator [26] that has been in clinical trials for psoriasis [27], topical treatment for human papillomavirus [28], prevention of infertility in chemotherapy patients [29] and for inhibition of angiogenesis [24, 30].

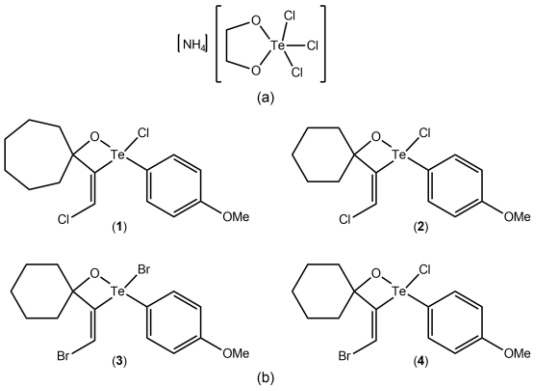

Fig. 1: Chemical diagrams of (a) ammonium trichlorido (dioxoethylene-O,O')tellurate (AS-101) and (b) (3E)-2-chloro-3-(chloromethylidene)-2-(4-methoxyphenyl)-1-oxa-2λ^4-telluraspiro-[3.6]decane (**1**), (3E)-2-chloro-3-(chloromethylidene)-2-(4-methoxyphenyl)-1-oxa-2λ^4-telluraspiro[3.5]nonane (**2**), and analogues of (**2**): the Te-bound bromido/methylidene-bromo species (**3**) and the mixed Te-bound chlorido/methylidene-bromo species (**4**).

Research on this non-toxic compound shows the cation to be a specific covalent inhibitor of cysteine proteases such as papain and Cathepsin B [26]. These observations have encouraged further studies of tellurium-

based compounds as inhibitors of this class of enzyme. In this context, Cunha and co-workers have presented series of organotellurium compounds that show irreversible inhibitory activity greater than AS-101 against Cathepsin B as well as being irreversible inhibitors against Cathepsins K, L and S [31, 32].

The inhibition of cysteine protease by tellurium compounds is due to a substitution reaction that follows the removal of a labile group bound to tellurium leading to the formation of a covalent Te–S bond with the thiolate-S atom of a Cys29 residue, i.e. Te–SG [33, 34]. The difference in Cathepsin inhibition values exhibited by the same compound arise owing to specific features of the various sub-sites in the enzyme which are responsible for the specificity of the protease [35, 36]. Thus, in order to design a powerful and specific Cathepsin inhibitor, it is of fundamental importance to have detailed knowledge of the features of each sub-site of each Cathepsin [37-39]. In addition, it is worth highlighting that this class of enzyme is related to several pathological processes such as osteoporosis (Cathepsin K) [40, 41], neurodegenerative disease (Cathepsin D) [42] and metastasis in several types of cancer (Cathepsins B, K, L and S) [43-45]. Hence, Cathepsins are promising targets for the treatment of such disorders [46].

With the aim to understand how potential therapeutic agents based on tellurium inhibit cysteine proteases, significant effort has been made to elucidate their binding modes and correlate them with inhibitory data [47-51]. Continuing this research, the present work targets to explain trends in previous published inhibitory data of a series of halotelluroxetanes, Figure 1, against Cathepsins B, K, L and S. New crystallographic data are presented for **1** and **4**, Figure 1, and docking studies of cationic ligands **1'-4'**, i.e. species corresponding to **1-4** but with a tellurium-bound halide removed, with the above-mentioned proteases. Moreover, to more fully understand the structural relationships between Cathepsins B, K, L and S, a sequential and structural alignment of these has been made using a molecular visualisation program.

Experimental

Synthesis and crystal growth

Compounds **1-4** were prepared as previously described [52]. In a typical reaction, a solution of the 3-hydroxy alkyne (11 mmol) in dry benzene (10 mL) was added to a suspension of *p*-methoxyphenyltellurium trichloride/bromide (10 mmol) in dry benzene (40 mL). The reaction mixture was refluxed for 8 h, during which the *p*-methoxyphenyltellurium trichloride was consumed, forming a clear, yellow solution. The resulting solution was cooled to room temperature, diluted with ethyl acetate and washed with a saturated NH_4Cl solution and brine. The solvent was evaporated under reduced pressure and the residue was quickly chromatographed on SiO_2, using CCl_4 and $CHCl_3$/MeOH (5:1) as eluents. The resulting oils that were isolated after chromatography were recrystallised from CH_2Cl_2 for **1** and $CHCl_3$/hexane for **2** and **4** to yield crystals suitable for X-ray analysis. The structure of **2** has already been described [52].

Crystal structure determination

Intensity data for **1** and **4** were measured at 293 K on an Enraf Nonius TurboCAD4 diffractometer using graphite-monochromatised MoKα radiation (λ = 0.71073 Å). Data processing and absorption corrections (ψ-scans) were accomplished with CAD4 Express [53] and XCAD4 [54]. Unit cell data, X-ray data collection parameters, and details of the structure refinement are given in Table 1. The structures were solved by Direct Methods using SIR92 [55] and full-matrix least-squares [56] refinement was on F^2 (anisotropic displacement parameters and C-bound H atoms in their idealised positions). A weighting scheme of the form $w = 1/[\sigma^2(F_o^2) + (aP)^2 + bP]$ where $P = (F_o^2 + 2F_c^2)/3$ was introduced. The programs WinGX [57], PLATON [58], ORTEP-3 for Windows [57] and DIAMOND [59] were also used in the study.

Tab: 1. Crystallographic data and refinement details for **1** and **4**.[1]

	1	**4**
Formula	$C_{16}H_{20}Cl_2O_2Te$	$C_{15}H_{18}BrClO_2Te$
Formula weight	442.82	473.25
Crystal colour, habit	Colourless, prism	Colourless, prism
Crystal size/mm	0.15 x 0.20 x 0.30	0.10 x 0.10 x 0.20
Crystal system	monoclinic	triclinic
Space group	$P2_1/c$	$P\bar{1}$
a/Å	9.4478(8)	9.2532(9)
b/Å	21.0267(10)	9.9010(10)
c/Å	9.3916(7)	10.1590(10)
α/°	90	96.080(10)
β/°	111.622(5)	92.621(9)
γ/°	90	116.370(10)
V/Å^3	1734.4(2)	824.68(16)
Z/Z'	4/1	2/1
D_c/g cm^{-3}	1.696	1.906
F(000)	872	456
μ(Mo$K\alpha$)/mm^{-1}	2.024	4.386
Measured data	5312	3503
θ range/°	2.3-30.0	2.5-26.3
Unique data	5040	3299
R_{int}	0.026	0.022
Observed data ($I \geq 2.0\sigma$	4036	2846
R, obs. data; all data	0.027; 0.046	0.023; 0.034
a, b in wghting scheme	0.032, 0.918	0.034, 0.418
R_w, obs. data; all data	0.068, 0.072	0.058; 0.061
$\Delta\rho_{max,\ min}$/e Å^{-3}	0.43, 0.81	0.32, 0.50

[1] Supplementary Material: Crystallographic data for the structures reported in this paper have been deposited with the Cambridge Crystallographic Data Centre as supplementary publication no. CCDC-1552738 and 1552739. Copies of available material can be obtained free of charge, on application to CCDC, 12 Union Road, Cambridge CB2 1EZ, UK, (fax: +44-(0)1223-336033 or e-mail: deposit@ccdc.cam.ac.uk).

Generation of ligand structures

To generate ligand structures for the docking studies, the experimentally determined structures of **1**, **2** and **4** were used as the starting points. The structures were made cationic by the removal of the tellurium-bound halide in each case, leading to **1'**, **2'** and **4'**, respectively, meaning the cation derived from **3** is equivalent to **4'**. Although the experimental structures uniformly have an E configuration about the exocyclic double bond, each was isomerised to have a Z configuration for trialling in the docking calculations. The HyperChem 8.0 program [60] was used for all manipulations with the Steepest Descent method and with a RMS gradient of 0.01 kcal / (Å mol).

Docking studies

The GOLD 5.0.1 program [61, 62] was used with the GoldScore fitness function that takes into account factors such as hydrogen-bonding energy, van der Waals energy and ligand torsion strain.

The performed calculations were based on the formation of a covalent complex involving the cysteine residue of the catalytic sites of the Cathepsins and the tellurium atom of the telluroxetanes.

Docking simulations were carried out considering the rigid enzyme and total ligand flexibility. Only amino acid residues within a radius of 10.0 Å around the ligand cavity were considered. All water molecules were removed since there are none in the active sites of the structures of the original Cathepsins and are therefore, not influential in the interactions.

y do not participate in the interactions between the ligand and enzyme.

The formation of a covalent bond between the sulphur atom of cysteine-reactive site SG (Cys29 in Cathepsin B and Cys25 in other Cathepsins) and the tellurium atom of each ligand was imposed. The constraint parameter of the GOLD program was employed to establish a range for the bond length between the tellurium and sulphur atom. The range used was 2.4 to 3.5 Å where the ligand has the freedom to settle in the active site of the enzyme.

Molecular visualization

For molecular visualization of the poses and for the analysis of interactions and alignments, the DS Visualizer program 3.5 [63] was employed.

Results

Experimental molecular structures

The molecular structure of **1** as determined by X-ray crystallography is shown in Figure 2 and selected geometric parameters are collated in Table 2. The immediate coordination geometry of the tellurium atom is defined by a chloride anion, an oxygen and two carbon atoms. Molecules self-assemble across a centre of inversion via secondary Te···O interactions to form dimeric aggregates. Hence, the tellurium atom is five-coordinate within a C_2ClO_2 donor set. The stereochemically active lone-pair of electrons is projected to occupy a position approximately trans to the Te-bound aryl substituent. The central $\{\cdots Te–O\}_2$ parallelogram has quite distinct

edge lengths of approximately 2.1 and 2.9 Å. Within the ring, short O1···O1^{i} contacts of 2.662(2) Å are noted; symmetry operation i: 1-*x*, -*y*, 1-*z*. The configuration about the C2=C3 double bond is E.

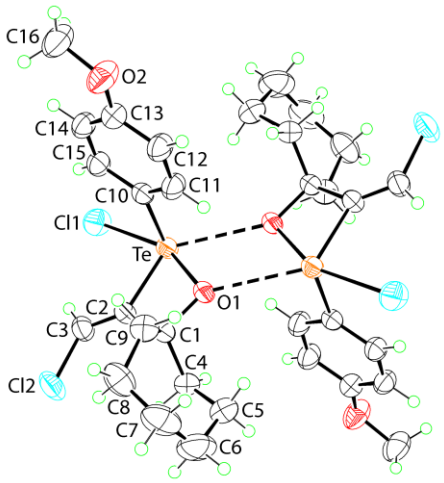

Fig. 2: Molecular structure of **1** showing atom labelling and displacement ellipsoids at the 50% probability level. Unlabelled atoms are related by the symmetry operation: 1-*x*, -*y*, 1-*z*.

Tab. 2: Summary of key geometric parameters (Å, º) for **1** and **4**[1]

Parameter	**1**; n = 10	**4**; n = 9
Te–C11	2.5556(7)	2.5309(9)
Te–O1	2.0440(17)	2.0574(19)
Te–C2	2.110(2)	2.107(3)
Te–C(n)	2.128(3)	2.122(3)
Te–O1^{i}	2.9039(17)	2.909(2)
C2–C3	1.314(3)	1.312(4)
Cl1–Te–O1	156.52(5)	156.71(6)
Cl1–Te–C2	90.11(7)	90.82(8)
Cl1–Te–C(n)	91.20(7)	90.62(8)
Cl1–Te–O1^{i}	141.08(4)	139.45(5)
O1–Te–C2	66.47(8)	66.04(10)
O1–Te–C(n)	91.64(8)	91.02(10)
O1–Te–O1^{i}	62.26(7)	63.71(8)
C2–Te–C(n)	100.43(9)	100.22(11)
C2–Te–O1^{i}	128.00(8)	128.41(9)
C(n)–Te–O1^{i}	89.26(7)	91.66(9)
Te–O1–C1	99.38(13)	98.69(15)
Te–C2–C1	94.66(14)	94.62(18)
Te–C2–C3	127.1(2)	127.4(2)
O1–C1–C2	99.35(18)	100.2(2)

[1] Symmetry operation i: **1** 1-*x*, -*y*, 1-*z* and **4** 1-*x*, 2-*y*, 2-*z*.

The four-membered ring comprising the Te, O1, C1 and C2 atoms is essentially planar [r.m.s. deviation = 0.0201 Å] with the deviations from

the least-squares plane being 0.0141(8), -0.0205(11), 0.0253(14) and -0.0189(10) Å, respectively. The seven-membered ring adopts a twisted chair conformation with the central C1, C4, C6, C7 and C9 atoms [r.m.s. deviation = 0.0820 Å; deviations = -0.030(2), 0.083(2), -0.114(3), 0.104(3) and -0.043(2) Å, respectively] defining the base with the C5 and C8 atoms lying 0.780(5) and 0.794(5) Å to either side of the base. The cycloheptane ring is twisted with respect to the 1,2-oxatelluretane ring with the dihedral angle between the best planes through each ring being 72.67(10)°, indicating an almost orthogonal arrangement. Indeed, the C1 atom lies in the plane of the oxatelluretane ring and the C6–C7 bond is bisected by the plane. The methyoxyphenyl ring lies perpendicular to the oxatelluretane ring as seen in the dihedral angle of 78.64(8)°.

In the molecular packing of **1**, the only specific contacts between molecules within the standard distance criteria in PLATON [58] is a C–Cl···π(arene) contact, i.e. C3–Cl2···Cg(C10-C15)^{ii} = 3.7069(15) Å, C3···Cg(C10-C15)^{ii} = 5.199(3) Å with the angle at Cl2 being 142.66(10)° for symmetry operation ii: 2-*x*, -*y*, 2-*z*. These interactions lead to supramolecular layers in the ac-plane, Figure 3a. Within the layers, very weak Te···Cl2^{iii} contacts are noted with the separation of 3.8505(10) Å being about 0.04 Å greater than the sum of their van der Waals radii [58]; symmetry operation iii: 2-*x*, -*y*, 1-*z*. The Cl2^{iii} atom approaches the tellurium centre from the unoccupied face and therefore, might be considered a weak chalcogen (secondary) bonding interaction [64]. The layers stack along the *b*-axis without directional interactions between them, Figure 3b.

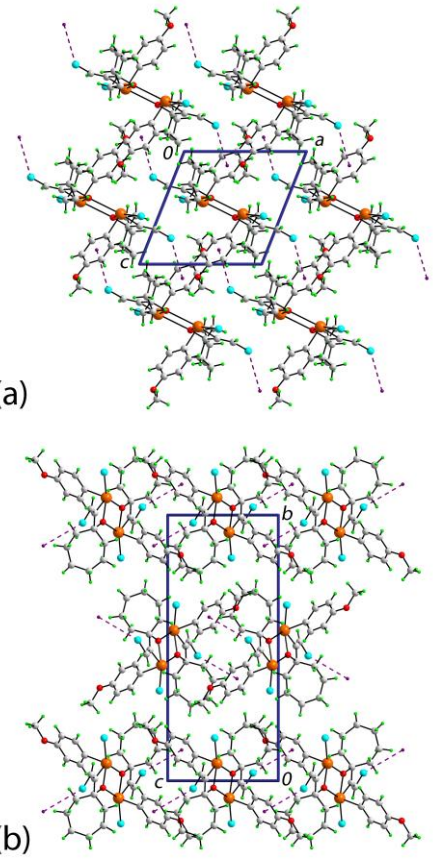

Fig. 3: Molecular packing in **1**: (a) view in projection down the *b*-axis of the unit cell showing the supramolecular layer sustained by C–H···Cl interactions and (b)

view of the unit cell contents down the *a*-axis highlighting the stacking of layers along the *b*-axis. The C–H···Cl interactions are represented as purple dashed lines.

The molecular structure of **4**, Figure 4, presents essentially the same features as just described for **1**, despite the presence of a six- rather than a seven-membered ring, and bromide at the C2=C3 double bond. Thus, the formation of a centrosymmetric, dimeric aggregate mediated by secondary Te···O interactions, the immediate tellurium atom coordination geometry and the E configuration of the double bond all persist. In terms of bond lengths, Table 2, there is a slight reduction in the Te–Cl bond length in **4**, by about 0.025 Å which appears to be compensated by a small elongation, i.e. 0.013 Å, in the Te–O bond. In the same way, variations in key bond angles are limited to about 2° and all involve the centrosymmetrically-related O1 atom with the maximum difference seen in the C(n)–Te–O1^{i} angles, i.e. 89.26(7) and 91.66(9)° for **1** and **4**, respectively. It is noted that the magnitude of the secondary Te···O interactions in both structures are equal within experimental error.

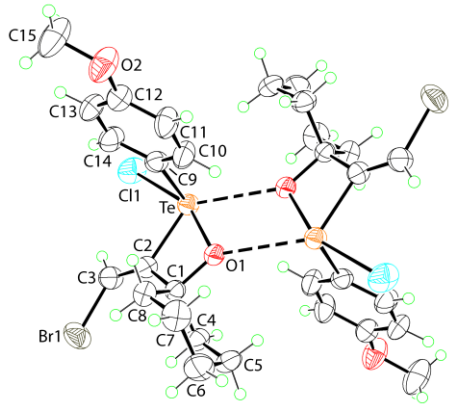

Fig. 4: Molecular structure of **4** showing atom labelling and displacement ellipsoids at the 50% probability level. Unlabelled atoms are related by the symmetry operation: 1-*x*, 2-*y*, 2-*z*.

The conformational relationships within the molecule of **4** match those for **1**. Thus, the oxatelluretane ring is planar [r.m.s. deviation = 0.0352 Å, with the deviations from the least-squares plane being -0.0242(8), 0.0357(12), -0.0446(15) and 0.0331(12) for Te, O1, C1 and C2 atoms, respectively]. The cyclohexyl ring has a chair conformation and the best-plane through this ring forms a dihedral angle of 87.98(12)° with the oxatelluretane ring indicating a twisted relationship analogous to that described for **1**. Finally, the oxatelluretane and methyoxyphenyl rings are perpendicular with the dihedral angle being 80.14(9)°.

The molecular packing of **4** exhibits C–Br···π(arene) contacts, i.e. C3–Br1···Cg(C9-C14)^{ii} = 3.7686(15) Å, C3···Cg(C9-C14)^{ii} = 5.275(4) Å with the angle at Br1 being 135.18(12)° for symmetry operation ii: -*x*, 1-*y*, 2-*z*. As shown in Figure 5a, these interactions lead to supramolecular layers in the ac-plane. Analogous to **1**, weak Te···Br1^{iii} chalcogen (secondary) bonding interactions within the layers are evident with the separation being 3.9179(6) Å, i.e. about 0.01 Å greater than the sum of their van der Waals radii [58]; symmetry operation iii: -*x*, 2-*y*, 2-*z*. The layers stack along the

c-axis without directional interactions between them. While not isomorphous, **1** and **4** are close to being isostructural having very similar molecular packing.

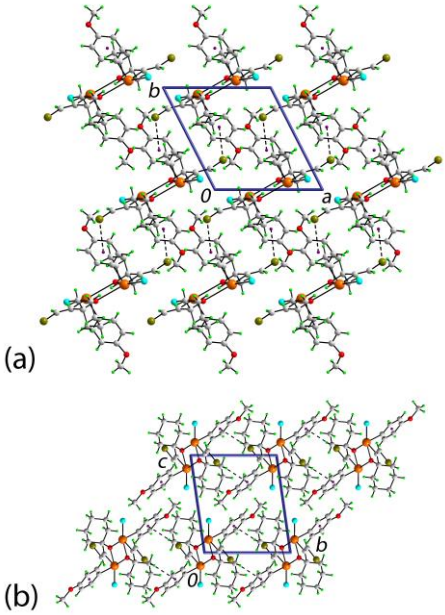

Fig. 5: Molecular packing in **4**: (a) view in projection down the *c*-axis of the unit cell showing the supramolecular layer sustained by C–H···Br interactions and (b) view of the unit cell contents down the *a*-axis highlighting the stacking of layers along the *c*-axis. The C–H···Br interactions are represented as purple dashed lines.

Docking studies

The enzymes used as molecular targets in the docking calculations were human Cathepsins B, K, L and S. Their three-dimensional structures were retrieved from the Protein Data Bank (PDB) [65] and PDBSum [66]. Their pdb codes and the resolution of their X-ray crystal structures are shown in Table 3.

Tab. 3: Three-dimensional features of the Cathepsins (Cat.) employed in the present study.

Enzyme	PDB code	Resolution	Reference
Cat. B	1GMY	1.9 Å	[67]
Cat. K	1U9V	2.2 Å	[68]
Cat. L	2XU3	0.9 Å	[69]
Cat. S	1MS6	1.9 Å	[70]

According to Schechter and Berger [71], the protease active sites of the papain family comprises sub-sites that are distinct in each protease and are crucial for their inhibition [37]. Since there is a lack of a complete description in the literature of the Cathepsin K, L and S sub-sites, it was necessary to perform a sequential and structural alignment of Cathepsins K, L and S with the aim of determining the residues comprising their sub-sites; Cathepsin B is well understood in this regard. The alignments were related to

the Cathepsin B residues, since this has the best description of sub-sites, as well as the classical catalytic triad residues of Cathepsins: cysteine, histidine and asparagine.

Experimental observations showed that tellurium(IV) compounds are irreversible inhibitors of cysteine proteases [28, 31, 72, 73]. The inhibition occurs due to the formation of a Te(IV)-SG covalent bond between the electrophilic tellurium(IV) centre and the nucleophilic thiol group of the catalytic cysteine via the loss of a leaving group bound to the tellurium atom [31, 32, 47, 48]. According to previous work [47, 48], to create an environment to satisfy the covalent complex hypothesis, the tellurium-bound halide, considered the best leaving group in each of **1**-**4**, was removed giving the corresponding cations **1'**, **2'**, **3'** and **4'**, respectively and these were used to simulate the formation of the Cathepsin-telluroxetane complexes in the enzymes listed in Table 3. It should be noted that after removing the tellurium-bonded halide **3'** is equivalent to **4'** so only **3'** was used for the final stages of the docking studies, i.e. when the Te–SG covalent bond is formed. Docking simulations were performed for each Cathepsin based on the formation of a covalent complex involving the E- and Z-isomers of each telluroxetane with the sulphur of the catalytic cysteine residue.

Structural and sequence alignments

It is well established that a potent and specific inhibitor against Cathepsins will have structural features that, besides interacting with the catalytic triad, will interact with regions called sub-sites that are responsible of the protease specificity [74] contributing to its stabilisation in that position. Table 4 summarises some sub-sites that according to the literature should be occupied for an efficient and specific inhibition. Herein, a brief overview of the relevant sub-sites in each studied Cathepsin is presented. It is important to highlight that in all cases the occupation of the S1 sub-site is required for inhibition, as this is the place where the catalytic thiol is located.

Tab. 4: Sub-sites that should be occupied to achieve the most efficient inhibition of the studied Cathepsins (Cat.).

Enzyme	Sub-sites	References
Cat. B	S1, S1', S2'	[75]
Cat. K	S1, S2, S3, S1'	[76]
Cat. L	S1, S2, S3, S1'	[77]
Cat. S	S1, S2, S3	[78-80]

From the structural and sequential alignment, it was possible to observe a significant structural similarity between the studied Cathepsins. As can be seen in Figure 6, there is a good overlap of α-helices and β-sheets, the difference being mainly in the loops of different conformations and sizes. Moreover, the amino acids sub-sites composition of Cathepsins B, K, L and S were determined, as shown in Table 5.

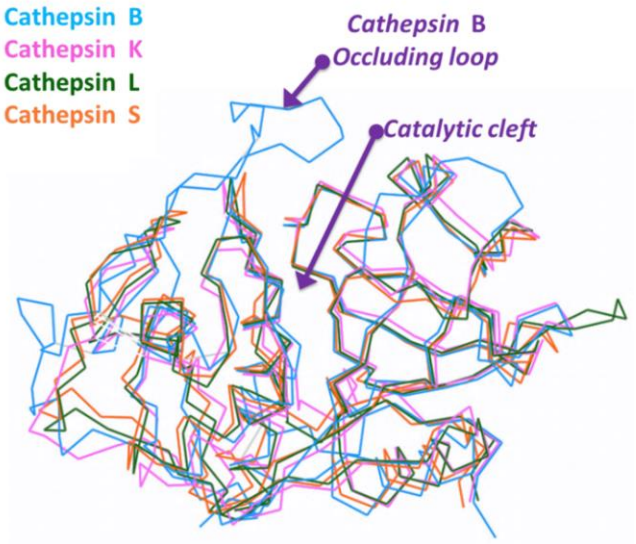

Fig. 6: Diagram showing the overlap, using the backbone trace line, of the three-dimensional structures of Cathepsins B (blue), K (pink), L (green) and S (orange) The Cathepsin B occluding loop is shown as this region gives exopeptidase activity to this protease, which is the only one that acts as an endo-/exo-peptidase [81-83].

Tab. 5: A summary of the residues that comprise the studied Cathepsin (Cat.) sub-sites and colour code for the sub-sites

Sub-site	Cat. B	Cat. K	Cat. L	Cat. S
S3	Tyr75	Tyr67 Glu59 Asp61	Gly61 Glu63 Asn66 Gly67 Leu69	Gly62 Lys64 Phe70
S2	Pro76 Ala173 Ala200 Glu245	Met68 Ala134 Ala163 Leu209	Met70 Ala135 Asp160 Met161 Gly164 Ala214	Met71 Gly137 Val162 Asn163 Gly165 Phe211
S1	Gln23 Gly27 Cys29 Gly74 Gly198	Gly23 Ser24 Cys25 Gly64 Gly65 Gly66 Asn161	Gln19 Gly23 Ser24 Cys25 Gly68	Gln19 Cys22 Gly23 Cys25 Cys66 Asn67 Gly68 Gly69
S1'	Val176 Phe180 Leu181 Met196 His199	Ala137 Gln143 Phe142 His162	Ala138 Gly139 Ser142 Leu144 His163 Trp189	Ala140 Arg141 Phe145 Phe146 His164 Trp186

S2'	Gly24 His110 His111 Gly121 Trp221	Gln19 Gly20 Trp184	Gln19 Gly20 Asp162	Gln19 Gly20 Trp186

Analyses of the Cathepsin-ligand complexes

Ligands **1'**, **2'** and **4'** were evaluated in both their E- and Z-configurations with all Cathepsins. The ligands with the six-membered alkane ring showed the best results for covalent bond formation rather than **1'** that has a seven-membered alkane ring, a result indicating steric hindrance associated with the increasing size of the ring.

For each study, docking results were first analysed by clustering similar poses. Within each group, the pose with the highest score and the shortest Te–SG distance was chosen, Table 6, then the interactions of the ligand-enzyme complex were analysed.

Tab. 6: Docking results for E- and Z-configurations of **1'**, **2'** and **4'** with the studied Cathepsins (Cat.). The most favourable distances and scores are highlighted in yellow.

E	**Cat. S**		**Cat. K**		**Cat. L**		**Cat. B**	
Ligand	Te–SG (Å)	score (kcal/mol)	Te–SG (Å)	score (kcal/mol)	Te–SG (Å)	score (kcal/mol)	Te–SG (Å)	score (kcal/mol)
1'	3.5	41.1	3.4	42.9	3.5	41.1	3.5	42.6
2'	3.0	48.0	3.0	43.1	2.9	42.4	3.0	40.0
3'	2.9	47.5	3.1	43.5	3.1	42.2	3.0	43.2
Z	**Cat. S**		**Cat. K**		**Cat. L**		**Cat. B**	
Ligand	Te–SG (Å)	score (kcal/mol)	Te–SG (Å)	score (kcal/mol)	Te–SG (Å)	score (kcal/mol)	Te–SG (Å)	score (kcal/mol)
1'	3.6	41.6	2.9	33.0	3.8	34.6	3.7	31.5
2'	3.4	42.3	5.4	40.7	2.9	38.2	4.3	36.1
3'	3.4	34.4	3.2	42.1	3.5	32.8	4.1	32.2

The analysis of the docking calculations indicates more favourable results for ligands having an E-configuration rather than Z (Table 6). For distances Te–SG > 3.2 Å, there is no covalent bond formation, which is in agreement with the very poor activity of **1** in Cathepsin B, Table 7. Further, as seen from the Supplementary Materials, the docked structures of **1'-3'** resemble very closely those observed in the molecular crystals structures with the obvious exception of the missing halide. This vindicates the assertion that GOLD [61, 62] indeed takes into account stereochemically-active lone-pairs of electrons as found in **1'-3'**.

Tab. 7: Second-order rate constant values (10^3 $M^{-1}s^{-1}$) for the inhibition of the studies Cathepsins (Cat.) by the telluroxetanes **1-3** [31, 32].

Compound	Cat. S	Cat. K	Cat. L	Cat. B
1	-	-	-	1.6 ± 0.1
2	196 ± 17	1200 ± 320	170 ± 12	36.0 ± 3.2
3	8940 ± 470	420 ± 31	650 ± 51	7.7 ± 0.9

The docking results for **2'** and **3'** (= **4'**) exhibit relatively small differences indicating that the halide has little influence on the activity. In Figure 7, the main amino acids residues interacting with the ligand molecules are indicated with further details given in the captions to Figs 8-11.

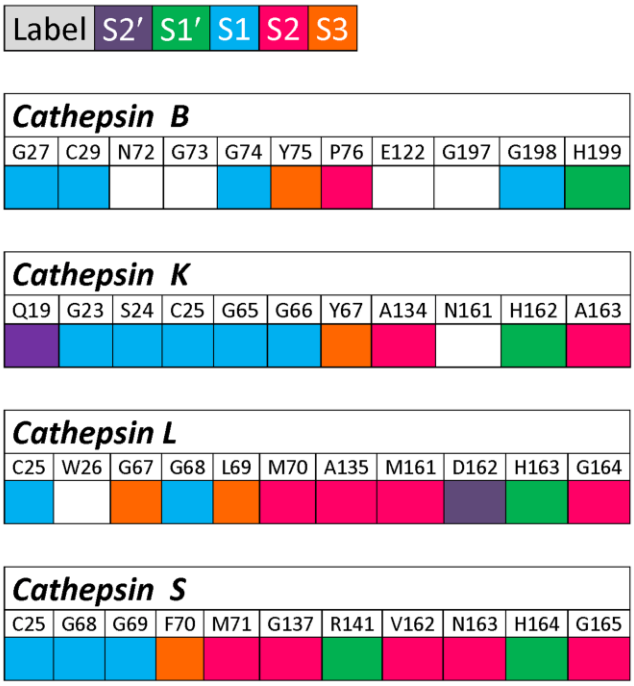

Fig. 7: A summary of the main interactions of ligands **2'** and **3'** in the studied Cathepsins. Colours follow that of Table 5, those not coloured refer to interactions not involving any specific subsite.

In the following, the surface representation of the best pose together with some interactions for ligands **2'** and **3'** in the four Cathepsins will be presented. The sub-sites colours for Figures 8-11 are defined as in Table 5.

In Figure 8a, the surface representation of the best pose of ligands **2'** and **3'** in Cathepsin B and in Figure 8b highlights the C–O···π interaction with Gly74 of sub-site S1 and the C–O···Te interaction with Gly27.

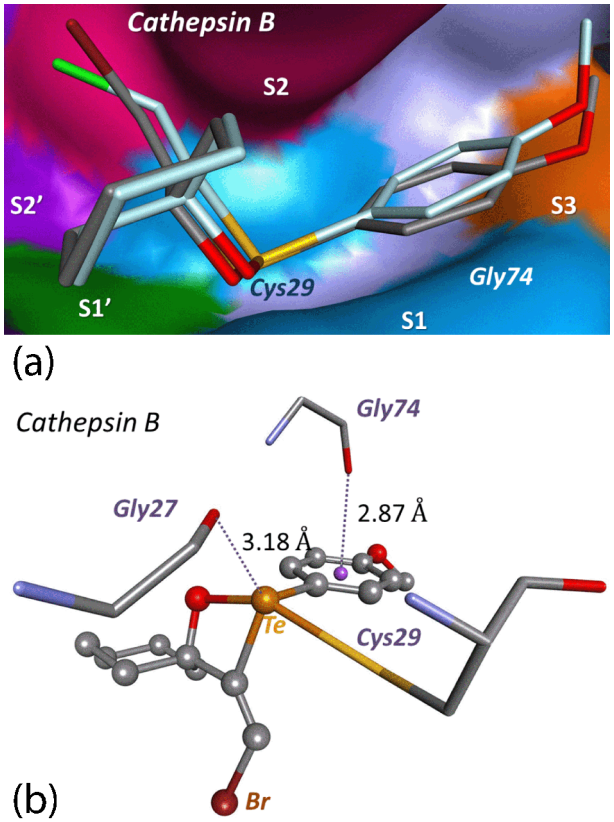

Fig. 8: (a) Surface representation of ligands **2'** and **3'** in the E-configuration in Cathepsin B and (b) two interactions of **3'** with residues of sub-site S1.

As indicated in Table 4, a good and specific Cathepsin B inhibitor should occupy the S1' and S2' sub-sites, especially the S2' sub-site which comprises the occluding loop that was shown to be very important for inhibition activity [48, 75]. The docking results, shown in Figure 7 for **2'** and **3'** in Cathepsin B indicate that these do not occupy the S2' sub-site and this may explain the fact of their very low binding affinity values for this protease, as indicated in Table 7.

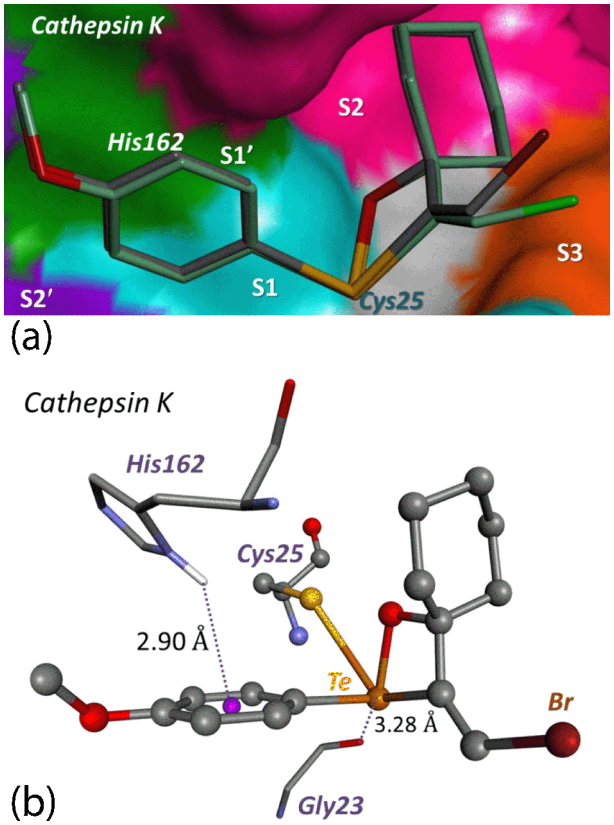

Fig. 9: (a) Surface representation of ligands **2'** and **3'** in the E-configuration in Cathepsin K and (b) two interactions of **3'** with residues of sub-sites S1 and S1'.

The docking studies in Cathepsin K shows that the telluroxetanes are positioned in the active site and occupy the S1, S1' and S2 sub-sites (Figures 7 and 9). These results explain the good Cathepsin K inhibition values of **2** and **3** (Table 7). Figure 9a shows the surface representation of the best poses of ligands **2'** and **3'** in Cathepsin K and in Figure 9b are shown two of the interactions involving **3'**: a C–H···π interaction with His162 from the S1' sub-site and a Te···O contact with Gly23 of the S1 sub-site.

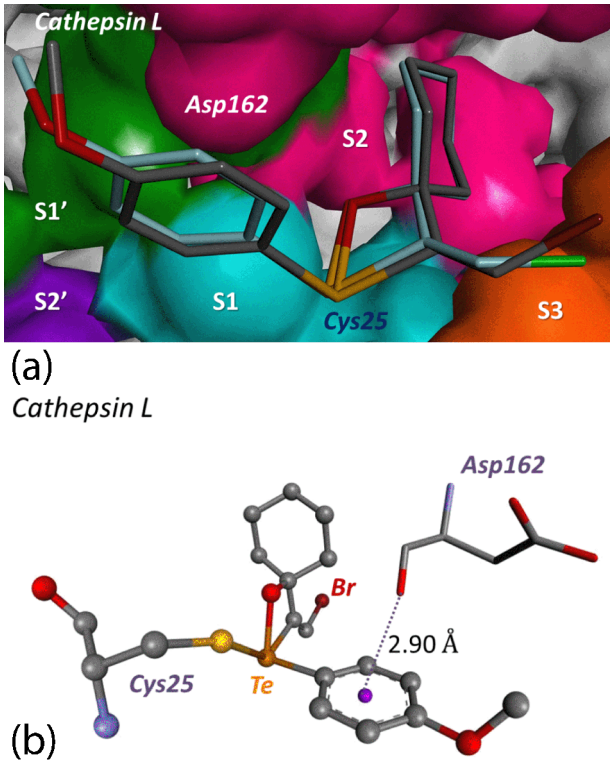

Fig. 10: (a) Surface representation of ligands **2'** and **3'** in the E-configuration in Cathepsin L and (b) the C–O···π interaction of **3'** with a residue of sub-site S2.

In Cathepsin L, the telluroxetane ligands occupy the S1, S1', S2 and S3 sub-sites (Figures 7 and 10), which can explain their relative good inhibition activity (Table 7). In this case, the shortest distance to the tellurium(IV) atom involves the oxygen of Gly68, i.e. at 3.92 Å.

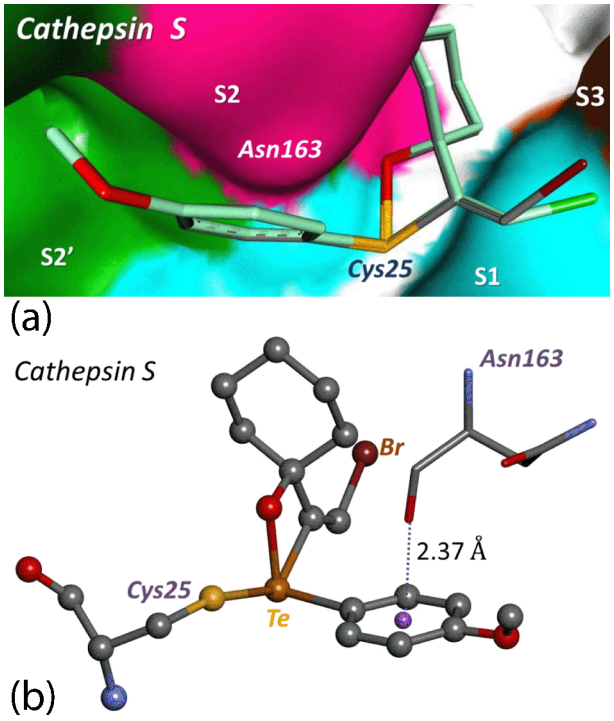

Fig. 11: Surface representation of ligands **2'** and **3'** in the E-configuration in Cathepsin S and (b) C–O···π interaction of **3'** with a residue of sub-site S2.

As seen in Figures 7 and 11a for Cathepsin S, ligands **2'** and **3'** are positioned in the S1, S1', S2 and S3 sub-sites, with the cyclohexane moiety located in the S2 sub-site. In this case, the shortest Te···O distance is from Gly69 at 3.93 Å. Furthermore, the occupation of the S2 and S3 sub-sites are described as crucial for Cathepsin S selectivity with respect to the other Cathepsins, especially Cathepsin K [78]. These results are in good agreement with the inhibitory activity observed for **2** and **3** as shown in Table 7.

Overview

The analysis of the docking calculations indicates more favourable results for ligands having an E-configuration rather than Z.

In each Cathepsin, ligands **2'** and **3'** have very similar binding modes, i.e. they form a Te–SG covalent bond and the phenyl ring makes a C–O…π interaction. The other interactions with other residues of different sub-sites are specific for each Cathepsin.

It is worth pointing out the different behaviour of the organic-ligand-bound halides. In Cathepsins B and K, these halides are not involved in any kind of interaction, whereas in Cathepsin L the Gly68 residue is involved in C–O···Cl halogen bond (2.65 Å) to the chloride atom of ligand **2'**, and with the bromide atom of ligand **3'**, at 3.50 Å, Figure 12. In Cathepsin S, the halides are involved in interactions with the phenyl ring of Phe70, the chloride forming a delocalised interaction and the bromine forming a localised interaction; see Figure 13.

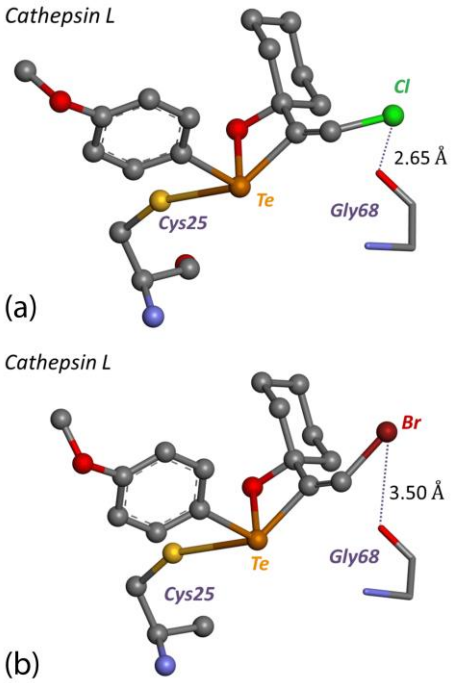

Fig. 12: (a) An image of the Cl···O halogen-bond formed by ligand **2'** and the Gly68 residue in Cathepsin L and (b) an analogous Br···O interaction between **3'** and Gly68.

Another interesting observation is the fact that when the halides are not involved in interactions as is the case with Cathepsins B and K, the second-order rate constant for inhibition for each complex is greater for the chloride-containing compound. Whereas with Cathepsins S and L, where the halides are involved in the interactions, shown in Figures 12 and 13, the relationship between the second-order rate constants is the opposite.

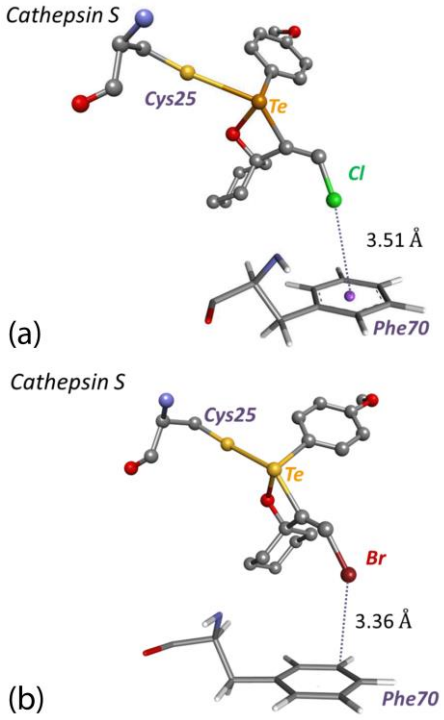

Fig. 13: (a) An image of the delocalised Cl···π interaction formed by ligand **2'** with the ring in Phe70 in Cathepsin S and (b) an analogous but localised Br···π interaction between **3'** and Phe70.

Conclusions

Biologically active tellurium/organotellurium compounds such as AS-101 and **1**-**4** are known to inhibit biologically important substrates such as Cathepsins. For **1**-**4**, there is loss of the tellurium-bound halide which enables the formation of covalent Te–SG bonds in most cases; the lack of a strong bond in the case of **1'** correlates with its relative lack of activity. Detailed docking studies confirms the relative importance of an E- over a Z- configuration in all cases. All Cathepsins studied feature a C–O···π interaction involving a phenyl ring for ligands **2'** and **3'** (= **4'**). Interestingly, the nature of organic residue-bound halide has no influence on the binding mode in Cathepsins B and K. By contrast, in Cathepsin L these atoms are involved in C–O···X halogen bonds, whereas in Cathepsin S, these halides form delocalised (chloride) and localised (bromide) interactions. This differential behaviour provides hope for the rational design of molecules to target specific receptor sites in Cathepsins.

In terms of future work, this study demonstrates the efficacy of E- over Z-configurations for the investigated tellurooxetanes, at least for Cathepsins B, K, L and S. Thus, the search for more promising inhibitors suggests the need of diastereoselective synthesis. Also, structural modifications are required so that metabolites of new test compounds can occupy subsite S3 of the active site of Cathepsin K, and should occupy all extensions of the active site of cathepsin L. Moreover, the poor inhibition activity and the docking results in Cathepsin B shows the need for chemical modifications

that will enable interaction with the S1' and S2' sites in the receptor site of Cathepsin B. Finally, for Cathepsin S, it seems important that more interactions are required with subsites S2 and S3.

Acknowledgements: The support of the Brazilian agencies the National Council for Scientific and Technological Development (CNPq-308480/2016-3 to IC, 305626/2013-2 to JZS), São Paulo Research Foundation (FAPESP-12/22524-9 to SHM) and the Coordination for the Improvement of Higher Education Personnel (CAPES) are acknowledged.

References

[1] J. T. Rotruck, A. L. Pope, H. E. Ganther, A. B. Swanson, D. G. Hafeman, W. G. Hoekstra, *Science* **1973**, *179*, 588.
[2] L. Flohé, W. A. Günzler, H. H. Schock, *FEBS Lett.* **1973**, *32*, 132.
[3] A. Böck, K. Forchhammer, J. Heider, J. Leinfelder, G. Sawers, B. Veprek, F. Zinoni, *Mol. Microbiol.* **1991**, *5*, 515.
[4] T. C. Stadtman, *Ann. Rev. Biochem.* **1996**, *65*, 83.
[5] J. Rafique, R. F. S. Canto, S. Saba, F. A. R. Barbosa, A. L. Braga, *Curr. Org. Chem.* **2016**, *20*, 166.
[6] D. Mániková, L. M. Letavayová, D. Vlasáková, P. Košík, E. C. Estevam, M. J. Nasim, M. Gruhlke, A. Slusarenko, T. Burkholz, C. Jacob, M. Chovanec, *Molecules* **2014**, *19*, 12258.
[7] L. Piovan, P. Milani, M. S. Silva, P. G. Moraes, M. Demasi, L. H. Andrade, *Eur. J. Med. Chem.* **2014**, *73*, 280.
[8] S. Shaaban, F. Sasse, T. Burkholz, C. Jacob, *Bioorg. Med. Chem. Lett.* **2014**, *22*, 3610.
[9] J. P. Johnpeter, G. Gupta, J. M. Kumar, Srinivas, G. N. Nagesh, B. Therrien, *Inorg. Chem.* **2013**, *52*, 13663.
[10] E. R. T. Tiekink, *Dalton Trans.* **2012**, *41*, 6390.
[11] C. W. Nogueira, G. W. Zeni, J. B. Rocha, *Chem. Rev.* **2004**, *104*, 6255.
[12] L. Orian, S. Toppo, *Free Radical Biol. Med.* **2014**, *66*, 65.
[13] G. Halpert, B. Sredni, *Autoimmun. Rev.* **2014**, *13*, 1230.
[14] R. H Revanna, R. K. Panchangam, U. Bhanu, S. Doddavenkatanna, *J. Braz. Chem. Soc.* **2016**, *27*, 1157.
[15] S. Kumar, L. Engman, L. Valgimigli, R. Amorati, M. G. Fumo, G. F. Pedulli, *J. Org. Chem.* **2007**, *72*, 6046.
[16] X. Ren, Y. Xue, J. Liu, K. Zhang, J. Zheng, G. Luo, C. Guo, Y. Mu, J. Shen, *ChemBioChem* **2002**, *3*, 356.
[17] S. E. C. Maluf, P. M. S. Melo, F. P. Varotti, M. L. Gazarini, R. L. O. R. Cunha, A. K. Carmona, *Parasitology Internat.* **2016**, *65*, 20.
[18] I. A. S. Pimentel, C. S. Paladi, S. Katz, W. A. S. Júdice, R. L. O. R. Cunha, C. L. Barbiéri, *PLoS ONE* **2012**, *7*, e48780.
[19] M. Brodsky, G. Halpert, M. Albeck, B. Sredni, *J. Inflammation*, **2010**, *7*, 3.
[20] D. Ling, B. Liu, S. Jawad, I. A. Thompson, C. N. Nagineni, J. Dailey, J. Chien, B. Sredni, R. B. Nussenblatt, *Br J Ophthalmol*. **2013**, *97*, 934.
[21] D. S. Avila, D. Colle, P. Gubert, A. S. Palma, G. Puntel, F. Manarin, S. Noremberg, P. C. Nascimento, M. Aschner, J. B. Rocha, F. A. Soares, *Toxicol. Sci.* **2010**, *115*, 194.
[22] B. Sredni, R. Geffen-Aricha, W. Duan, M. Albeck, F. Shalit, H. M. Lander, N. Kinor, O. Sagi, A. Albeck, S. Yosef, M. Brodsky, D. Sredni-Kenigsbuch, T. Sonino, D. L. Longo, M. P. Mattson, G. Yadid, G. *Faseb J.* **2007**, *21*, 1870.
[23] P. Du, N. E. B. Saidu, J. Intemann, C. Jacob, M. Montenarh, *Biochim. Biophys. Acta* **2014**, *1840*, 1808.
[24] H. L. Seng, E. R. T. Tiekink, *Appl. Organometal. Chem.* **2012**, *26*, 655.

[25] B. Sredni, *Semin. Cancer Biol.* **2012**, *22*, 60.
[26] A. Silberman, Y. Kalechman, S. Hirsch, Z. Erlich, B. Sredni, A. Albeck, *ChemBioChem* **2016**, *17*, 918.
[27] B. Sredni, R. R. Caspi, A. Klein, Y. Kalechman, Y. Danziger, M. Benyaakov, T. Tamari, F. Shalit, M. Albeck, *Nature* **1987**, *330*, 173.
[28] A. Albeck, H. Weitman, B. Sredni, M. Albeck, *Inorg. Chem.* **1998**, *37*, 1704.
[29] M. Friedman, I. Bayer, I. Letko, R. Duvdevani, O. Zavaro-Levy, B. Ron, M. Albeck, B. Sredni, *Br. J. Dermatol.* **2009**, *160*, 403.
[30] L. Kalich-Philosoph, H. Roness, A. Carmely, M. Fishel-Bartal, H. Ligumsky, S. Paglin, I. Wolf, H. Kanety, B. Sredni, D. Meirow, *Sci. Transl. Med.* **2013**, *5*, 185.
[31] R. L. O. R. Cunha, M. E. Urano, J. R. Chagas, P. C. Almeida, C. Bincoletto, I. L. S. Tersariol, J. V. Comasseto, *Bioorg. Med. Chem. Lett.* **2005**, *15*, 755.
[32] R. L. O. R. Cunha, I. E. Gouvea, L. Juliano, L. *An. Acad. Bras. Cienc.* **2009**, *81*, 393.
[33] S. Yosef, M. Brodsky, B. Sredni, A. Albeck, M. Albeck, *ChemMedChem* **2007**, *2*, 1601.
[34] A. Silberman, M. Albeck, B. Sredni, A. Albeck, *Inorg. Chem.* **2016**, *55*, 10847.
[35] Li, Y. Y., Fang, J., Ao, Z. G. *Expert Opin. Ther. Pat.* 2017, *27*, 643.
[36] M. Siklos, M. BenAissa, G.R.J. Thatcher, *Acta Pharm. Sin. B* **2015**, *5*, 506.
[37] B. Turk, *Nat. Rev. Drug Discov.* **2006**, *5*, 7.
[38] C. Palermo, J. A. Joyce, *Trends Pharmacol. Sci.* **2008**, *29*, 22.
[39] V. Turk, V. Stoka, O. Vasilijeva, M. Renko, T. Sun, B. Turk, D. Turk, D. *Biochim. Biophys. Acta, Proteins Proteomics*, **2012**, *1824*, 68.
[40] J. F. Charles, A. O. Aliprantis, *Trends Mol. Med*., **2014**, *20*, 449.
[41] D. Bromme, P. Panwar, S. Turan, *Expert Opin. Drug Discov.* **2016**, *11*, 457.
[42] V. Stoka, V. Turk, B. Turk, *Ageing Res. Rev.* **2016**, *32*, 22.
[43] M. Z. I. Pranjol, N. Gutowski, M. Hannemann, J. Whatmore, *Biomolecules* **2015**, *5*, 3260.
[44] U. Verbovsek, U. C. J. F. Van Noorden, T. T. Lah, *Semin. Cancer Biol.* **2015**, *35*, 71.
[45] O. C. Olson, J. A. Joyce, *Nat. Rev. Cancer* **2015**, *15*, 712.
[46] H. Appelqvist, P. Wäster, K. Kågedal, K. Öllinger, *J. Mol. Cell Biol.* **2013**, *5*, 214.
[47] R. L. O. R. Cunha, J. Zukerman-Schpector, I. Caracelli, J. V. Comasseto, *J. Organomet. Chem.* **2006**, *691*, 4807.
[48] I. Caracelli, J. Zukerman-Schpector, S. H. Maganhi, H. A. Stefani, R. Guadagnin, E. R. T. Tiekink, *J. Braz. Chem. Soc.* **2010**, *21*, 2155.
[49] S. D. Ramalho, L. R. F. De'Sousa, L. Nebo, S. H. Maganhi, I. Caracelli, J. Zukerman-Schpector, M. I. S. Lima, M. F. M. Alves, M. F. G. F. Da'Silva, J. B. Fernandes, P. C. Vieira, *Chem Biodivers.* **2014**, *11*, 1354.
[50] I. Caracelli, M. Vega-Teijido, J. Zukerman-Schpector, M. H. S. Cezari, J. G. S. Lopes, L. Juliano, P. S. Santos, J. V. Comasseto, R. L. O. R. Cunha, E. R. T. Tiekink, *J. Mol. Struct.* **2012**, *1013*, 11.
[51] I. Caracelli, J. Zukerman-Schpector, L. S. Madureira, S. H. Maganhi, H. A. Stefani, R. C. Guadagnin, E. R. T. Tiekink, *Z. Kristallogr.* **2016**, *231*, 321.
[52] J. V. Comasseto, H. A. Stefani, A. Chieffi, J. Zukerman-Schpector, *Organometallics* **1991**, *10*, 845.
[53] CAD4 Express Software. Enraf-Nonius, Delft, The Netherlands, **1994**.

[54] XCAD4 - CAD4 Data Reduction. Harms, K. and Wocadlo, S. XCAD-4. Program for Processing CAD-4 Diffractometer Data. University of Marburg, Germany, **1995**.
[55] A. Altomare, G. Cascarano, C. Giacovazzo, A. Guagliardi, *J. Appl. Crystallogr*. **1993,** *26*, 343.
[56] G. M. Sheldrick, *Acta Crystallogr. A* **2008**, *64*, 112.
[57] L. J. Farrugia, *J. Appl. Crystallogr*. **2012**, *45*, 849.
[58] A. L. Spek, *J. Appl. Crystallogr*. **2003**, *36*, 7.
[59] K. Brandenburg, DIAMOND. Crystal Impact GbR, Bonn, Germany, **2006**.
[60] HyperChem(TM) Professional 7.51, Hypercube, Inc, 1115 NW 4th Street, Gainsville, Florida 32601, USA, **2015**.
[61] G. Jones, P. Willett, R. C. Glen, A. R. Leach, R. Taylor, *J. Mol. Biol.* **1997**, *267*, 727.
[62] G. Jones, P. Willett, R. C. Glen, *J. Mol. Biol.* **1995**, *245*, 43.
[63] Accelrys DS Visualizer v3.5 (http://accelrys.com/).
[64] E. R. T. Tiekink, *Coord. Chem. Rev*. **2017**, *345*, 209.
[65] PDB: http://www.rcsb.org/pdb/home/home.do
[66] PDBSum: http://www.ebi.ac.uk/pdbsum/
[67] P. D. Greenspan, K. L. Clark, R. A. Tommasi, S. D. Cowen, L. W. Mcquire, D. L. Farley, J. H. Duzer, R. L. Goldberg, H. Zhou, Z. Du, J. J. Fitt, D. E. Coppa, Z. Fang, W. Macchia, L. Zhu, M. P. Capparelli, R. Goldstein, A. M. Wigg, J. R. Dougthy, R. S. Bohacek, A. K. Knap, *J. Med. Chem.* **2001**, *44*, 4524.
[68] E. Altmann, S. W. Cowan-Jacob, M. Missbach, *J. Med. Chem.* **2004**, *47*, 5833.
[69] L. A. Hardegger, B. Kuhn, B. Spinnler, L. Anselm, R. Ecabert, M. Stihle, B. Gsell, R. Thoma, J. Diez, J. Benz, J. M. Plancher, G. Hartmann, D. W. Banner, W. Haap, F. Diederich, *Angew. Chem. Intl. Ed*. **2011**, *50*, 314.
[70] Y. D. Ward, D. S. Thomson, L. L. Frye, C. L. Cywin, T. Morwick, M. J. Emmanuel, R. Zindell, D. McNeil, Y. Bekkali, M. Girardot, M. Hrapchak, M. Deturi, K. Crane, D. White, S. Pav, Y. Wang, M. Hao, C.A. Grygon, M.E. Labadia, D. M. Freeman, W. Davidson, J. L. Hopkins, M. L. Brown, D. M. Spero, *J. Med. Chem*. **2002**, *45*, 5471.
[71] I. Schechter, A. Berger, *Biochem. Biophys. Res. Commun*. **1967**, *27*, 157.
[72] I. E. Gouvea J. A. N. Santos, F. M. Burlandy, I. L. S. Tersariol, E. E. Da'Silva, M. A. Juliano, L. Juliano, R. L. O. R. Cunha, *Biol. Chem.* **2011**, *392*, 587.
[73] L. Piovan, M. F. M. Alves, L. Juliano, D. Brömme, R. L. O. R. Cunha, L. H. Andrade, *Bioorg. Med. Chem. Lett.* **2011**, *19*, 2009.
[74] M. Drag, G. S. Salvesen, *Nat. Rev. Drug Discovery* **2010**, *9*, 690.
[75] D. Watanabe, A. Yamamoto, K. Tomoo, K. Matsumoto, M. Murata, K. Kitamura, T. Ishida, *J. Mol. Biol*. **2006**, *362*, 979.
[76] F. Lecaille, D. Brömme, G. Lalmanach, *Biochimie* **2008**, *90*, 208.
[77] M. C. Myers, P. P. Shah, M. P. Beavers, A. D. Napper, S. L. Diamond, A. B. Smith, D. M. Huryn, *Bioorg. Med. Chem. Lett.* **2008**, *18*, 3646.
[78] S. Yesa, C. Lindquist, T. Agback, K. Benkestock, B. Classon, I. Henderson, E. Hewitt, K. Jansson, A. Kallin, D. Sheppard, B. Samuelsson, *Bioorg. Med. Chem.* **2009**, *17*, 1307.
[79] D. Brömme, P. R. Bonneau, P. Lachance, A. C. Storer, *J. Biol. Chem.* **1994**, *269*, 30238.
[80] T. A. Pauly, T. Sulea, M. Ammirati, J. Sivaraman, D. E. Danley, M. C. Griffor, A. V. Kamath, I.-K. Wang, E. R. Laird, A. P. Seddon, R. Ménard, M. Cygler, V. L. Rath, *Biochemistry* **2003**, *42*, 3203.

[81] C. Illy, O. Quraishi, J. Wang, E. Purisima, T. Vernet, J. S. Mort, *J. Biol. Chem.* **1997**, *272*, 1197.
[82] J. C. Krupa, S. Hasnain, D. K. Nägler, R. Ménard, J. S. Mort, *Biochem. J.* **2002**, *361*, 613.
[83] M. Renko, U. Požgan, D. Majera, D. Turk, *FEBS J.* **2010**, *277*, 4338.
[84] M. F. M. Alves, L. Puzer, S. S. Cotrin, M. A. Juliano, L. Juliano, D. Brömme, A. K. Carmona, *Biochem. J*. **2003**, *373*, 981.
[85] S. F. Chowdhury, L. Joseph, S. Kumar, S. R. Tulsidas, S. Bhat, E. Ziomek, R. Ménard, J. Sivaraman, E. O. Purisima, *J. Med. Chem.* **2008**, *13*, 1361.